Effect of thiosulfate on pitting corrosion of Ni-Cr-Fe alloys in chloride solutions

Abraham A. Becerra Araneda,[*,**] Mariano A. Kappes,[*,**,***] Martín A. Rodríguez, [*,**,***] and Ricardo M. Carranza[*,**]

**Instituto Sabato, UNSAM/CNEA, Av. Gral. Paz 1499, San Martín, Buenos Aires, B1650KNA, Argentina.*

***National Commission of Atomic Energy of Argentina, Av. Gral. Paz 1499, San Martín, Buenos Aires, B1650KNA, Argentina.*

****National Scientific and Technical Research Council, Godoy Cruz 2290, Autonomous City of Buenos Aires, C1425FQB, Argentina.*

ARTICLE INFO (THIS STYLE IS ARTICLE AND ABSTRACT HEADING)

Article history: (This style is Article Info subhead)

Received Day Month Year (This style is Article History and Keywords)
Accepted Day Month Year
Available Day Month Year

Keywords:

A. Alloys 600, 690 and 800
B. Localized corrosion
C. Thiosulfate

*Place the contact information here. The format should be: Affiliation, Mailing Address, City, State Zip.

**The style is named contact.

***Corresponding author: telephone no; fax no.
Email: (e-mail: name@domain.edu).

ABSTRACT

Pitting corrosion of alloys 600, 690, and 800 (UNS N06600, N06690 and N08800) was studied in 1 M NaCl solution with different concentrations of thiosulfate ($S_2O_3^{2-}$). Alloys exhibited vastly different electrochemical behavior, depending on the $S_2O_3^{2-}$ concentration and chromium content of the alloy. Alloy 600 exhibited a breakdown and repassivation potential that decreased with decreasing $S_2O_3^{2-}$ concentration, in the range from 1 M to 10^{-4} M. Breakdown and repassivation potentials decreased about 300 and 600 mV, respectively, when 10^{-4} M $S_2O_3^{2-}$ was added to a 1 M NaCl solution. For alloys 690 and 800, additions of $S_2O_3^{2-}$ in the range of 1 M to 0.01 M caused a decrease in the breakdown and repassivation potentials. Dilute solutions were more aggressive, and a 0.01 M addition of thiosulfate to a 1 M NaCl solution caused a decrease in breakdown and repassivation potentials of about 300 mV. In a solution containing 0.001 M $Na_2S_2O_3$ + 1 M NaCl, alloys 690 and 800 showed two different submodes of pitting, each one of them existing at a different range of potential. Chloride pitting corrosion was observed at high potentials, and was characterized by pits with a lacy cover. The stable pit initiation potential associated with this process in both alloys was near 300 $mV_{Ag/AgCl}$, and was preceded by frequent metastable events. Chloride plus thiosulfate pitting was observed at low potentials (near -225 $mV_{Ag/AgCl}$) and was characterized by hemispherical pits. In potentiodynamic curves, this submode of pitting showed a characteristic anodic peak of approximately 120 mV width, and a maximum current density of 10 $\mu A/cm^2$ for both alloys. Potentiostatic tests at potentials within this anodic peak led to stable pit growth. Those pits could be repassivated by scanning the potential either in noble or active directions. Low potential and high potential pitting submodes were separated by a stable passivity range, as determined by potentiondynamic curves. Upon a further decrease in $S_2O_3^{2-}$ concentration down to 10^{-4} M, only high potential pitting corrosion was observed, with pitting and repassivation potentials similar than those in 1 M NaCl solution.

INTRODUCTION

It is currently accepted that thiosulfate ($S_2O_3^{2-}$) is an aggressive anion that can promote localized corrosion and stress corrosion cracking in stainless steels and corrosion-resistant alloys.[1] Thiosulfate can be present in a variety of environments, including paper-machine white water,[2] and in heat exchangers, where sulfate reducing bacteria (SRB) reduces sulfate (SO_4^{2-}) ions to H_2S that is then further oxidized in air to $S_2O_3^{2-}$.[3] In nuclear power plants, sulfate (SO_4^{2-}) is a common impurity found in steam generator secondary water that can be reduced to $S_2O_3^{2-}$ by action of hydrazine (N_2H_4), this last one added to secondary water to prevent corrosion of structural materials.[4] Previous work shows that thiosulfate promotes pitting corrosion in UNS N06600 (alloy 600)[5–8], N06690 (alloy 690)[6,9] and N08800 (alloy 800)[5,6,10–12] currently used in steam generator tubing and in other heat exchangers[3] of nuclear power plants.

Thiosulfate promotes pitting corrosion by reducing itself on the metal surface to form an adsorbed sulfur (S) or sulfide (S^{2-}) layer,[13] which prevents repassivation.[2] The thermodynamics of $S_2O_3^{2-}$ reduction to yield sulfur layers (S_{ads}) has been studied by Marcus and Protopopoff [14]. Those authors constructed potential-pH diagrams considering two-dimensional adsorbed sulfur layers. Those two-dimensional S_{ads} layers might be stable in regions where conventional Pourbaix diagrams, which consider three-dimensional compounds, do not predict formation of metal sulfides. S_{ads} layers are stable in a broad region of pH and potential when deposited on iron (Fe), nickel (Ni) or chromium (Cr). For a pH of about 2, representative of acid solutions inside sulfate-thiosulfate pits,[15] and a bulk dissolved sulfur concentration of 10^{-4} mol/kg, S_{ads} dominates in the potential range from -600 to 400 mV_{SHE} for a pure Fe substrate at 25°C.[14] A similar behavior is exhibited for Ni and Cr, with Ni having the largest S_{ads} stable zone. S_{ads} stable region overlaps with the passive domains of Fe, Ni and Cr, thus explaining why it hinders passivation or repassivation.[14,16]

Pitting corrosion in $S_2O_3^{2-}$ solutions requires the presence of a larger concentration of a strong acid anion, like chloride (Cl^-), sulfate or perchlorate (ClO_4^-),[13,15] so that one of those is the predominant anion at pit bottoms. Otherwise, pit stabilization can be prevented by proton consumption in thiosulfate disproportionation (Equation 1) or reduction (Equation 2) reactions.[6]

$$S_2O_3^{2-} + H^+ \rightarrow HSO_3^- + S \quad (1)$$

$$S_2O_3^{2-} + 6H^+ + 4e^- \rightarrow 3H_2O + 2S \quad (2)$$

Considering these reactions, it can be explained why thiosulfate pitting corrosion in sulfate solutions occurs for certain $[SO_4^{2-}]/[S_2O_3^{2-}]$ ratios: if too little thiosulfate is added, not enough S is deposited at the metal surface, but if too much thiosulfate is present it can neutralize the pit solution.[13]

Pitting corrosion in sulfate/thiosulfate solutions occurs within a narrow potential range.[6,15] At those intermediate potentials, both reduction of thiosulfate to S_{ads} that prevents repassivation, and anodic dissolution of metal required to maintain the critical acidification in the pit solution, can occur at optimum rates.[15] Therefore, pits in sulfate/thiosulfate solutions can repassivate when polarized at potentials either above or below the pitting susceptibility range.

On the contrary, for stainless steels, pits nucleated in chloride-thiosulfate solutions do not repassivate when polarized at intermediate potentials because thiosulfate pitting merges with chloride pitting.[9,13,17,18] Pitting corrosion in chloride-thiosulfate solutions has been studied extensively in stainless steels[5,12,17-19] and alloy 600.[8,20,21] It is generally agreed that maximum pitting corrosion susceptibility occurs at an intermediate $[Cl^-]/[S_2O_3^{2-}]$ ratio, which is in agreement with the mutual requirement of enough sulfur at pit bottoms, but still scarce so that repassivation by reactions 1 and 2 is prevented. The exact ratio reported by different investigators depends on the chemical composition of the studied alloy, chloride concentration and temperature.[17,22] Alloy 600, with a lower chromium content, appears to be less resistant to pitting corrosion in $[Cl^-]/[S_2O_3^{2-}]$ solutions than stainless steel 304 (UNS S30400), in the sense that more dilute thiosulfate solutions can considerably affect pitting potentials.[6,7] Thiosulfate can also decrease the stability of passive films and promote pitting corrosion of alloys 800 and 690, despite their higher chromium contents with respect to alloy 600.[5,9,23] The $[Cl^-]/[S_2O_3^{2-}]$ ratio for the maximum pitting corrosion susceptibility increases as the wt. % Ni of the alloys increases.[5]

Unlike lower chromium alloys, where thiosulfate-assisted pitting at low potential merges with chloride pitting at higher potential,[9,13,17,18] it was recently reported that alloys 690 and 800 can exhibit two different "submodes" of pitting in certain thiosulfate + chloride solutions.[24] The term "submode" in this paper is used according to the definition given by Staehle.[25] Examples of modes of corrosion, alternatively known as forms of corrosion[26, 27], are uniform corrosion, pitting corrosion, intergranular corrosion, stress corrosion cracking (SCC) and corrosion fatigue. Some modes of failure, like stress corrosion cracking in water at high temperature, comprise several submodes, as explained extensively by Staehle.[25] Each submode of SCC is characterized by certain kinetics of crack growth that depends on a specific way on the principal variables. For SCC, principal variables are potential, pH, species in the environment, temperature, stress, alloy structure and alloy composition. This phenomenological description makes possible quantitative predictions extremely valuable for engineering purposes, without any speculation on the mechanism or atomic process responsible for crack advance. In a first approximation, it can be accepted that the same principal variables that control SCC (with the likely exception of stress) control kinetics of pit growth. A change in a given principal variable can decrease the kinetics of a given submode while increasing the kinetics of another submode, several examples of this situation are detailed elsewhere for SCC of steam generator tubing alloys.[4,28]

While most cases of pitting attack reported in the literature exhibit a kinetics that increases with an increase in electrochemical potential, it is showed in this work that alloys 690 and 800 have a submode of pitting where pits can repassivate upon an *increase* in potential, hence the need of using the word "submode". For alloys 690 and 800, two different submodes of pitting failure were observed when small amounts of thiosulfate (0.001 M) were added to a 1 M NaCl solution[24]. Low potential pitting corrosion was observed at a potential about -160 $mV_{Ag/AgCl}$. High potential pitting corrosion initiated at a potential about 300 $mV_{Ag/AgCl}$ in 1 M NaCl solutions, and was not appreciably affected by small $S_2O_3^{2-}$ additions. In this work, these two pitting submodes will be investigated with different electrochemical techniques, highlighting their singularities. Tests were conducted at room temperature; hence, they are relevant for steam generators in lay-up conditions, where sulfur species and oxygen might be present. Previous work[3,6] shows that these are aggressive conditions, leading to localized corrosion of steam generator tubing alloys.

EXPERIMENTAL PROCEDURE

Alloys and Heat Treatments

The chemical composition of the studied alloys was obtained by X-ray fluorescence analysis, Table 1. Specimens were prepared from wrought mill annealed plate stock. Approximate dimensions of the specimens were 325 mm x 10 mm x 3 mm. Each alloy was solution annealed (SA) and aged (A) according to details in Table 2. In accord with previous work[29], grain boundaries are free from carbides after SA heat treatment, Figure 1, and carbides precipitated preferentially at grain boundaries in a nanometric scale after aging heat treatments (SA+A). The heat treatment SA + A is the recommended for alloys 600 and 690 steam generator tubing.[30,31] SA + A treatment was also performed to alloy 800 for comparative purposes with the other alloys although its application is not currently specified for this alloy for construction of steam generator tubes.

Electrochemical Tests

A conventional three-electrode borosilicate-glass cell was used. The cell volume was approximately 600 cm^3 and it was filled with 250 cm^3 of testing solution. The electrochemical cell was placed within an earth-grounded Faraday cage throughout the tests to minimize current noise pick up. A KCl saturated silver/silver chloride (Ag/AgCl) reference electrode ($E_{Ag/AgCl}$ = 0.198 V_{NHE}) was connected to the solution through a Luggin probe. The counter electrode was a platinum (Pt) foil with an area of approximately 20 cm^2.

Tests were performed at room temperature and atmospheric pressure. Three repetitions were performed for each testing condition. Testing solutions were 1 M NaCl with and without $Na_2S_2O_3$ additions from 0.0001 to 1 M. Solutions were prepared with analytical grade reagents and ultrapure water (resistivity of 18.2 MΩ.cm at 25°C). High purity (> 99.999%) nitrogen (N_2) was purged through the testing solution from 1 hour previous until the end of every test. Prior to all tests, the open circuit potential (E_{CORR}) was measured for 15 minutes.

Alloy specimens were ground down to 600 grit silicon carbide (SiC) emery paper and then washed in high-purity water and ethanol. Specimens were partially submerged in the solution in order to avoid the formation of undesired crevices. A platinum wire was used as an electrical contact and also to hang the specimens, thus setting the desired immersion level (exposed area). The submerged area was 3.0 cm^2. All the specimens were microscopically examined after testing. Corrosion damage morphology was characterized by Optical

Microscopy (OM) and Scanning Electron Microscopy (SEM) accompanied by elemental mapping by Energy Dispersive Spectroscopy (EDS).

Cyclic Potentiodynamic Polarization (CPP) tests were performed to characterize the electrochemical behavior of the alloys in the different solutions. Pitting (E_P) and repassivation (E_{RP}) potentials were determined by inspection of those curves. E_P was determined at the inflexion point of the forward anodic polarization curve and E_{RP} was determined at the cross-over of the forward and reverse potential scans. The potential scan rate was 0.167 mV/s. The scan started 50 mV below E_{CORR}, and it was reversed from anodic to cathodic when the current density reached 1 mA/cm^2.

Sets of potentiostatic (PS) tests were performed in 1 M NaCl and 1 M NaCl + 0.001 M $Na_2S_2O_3$ solutions. PS tests consisted of a series of 10-mV potentiostatic steps from E_{CORR} to 0.6 $V_{Ag/AgCl}$. Every potential step lasted 20 minutes unless the recorded current density was higher than 30 µA/cm^2. In such a case the following potential step was applied (a 10-mV increase) until the current density dropped below 30 µA/cm^2, which was a possible scenario because pits in thiosulfate solutions can repassivate if polarized to a potential above its range of stability. The maximum current density measured in every step was plotted vs. applied potential and the obtained curve was compared to a potentiodynamic curve, performed at a scan rate of 0.167 mV/s. Localized corrosion is frequently observed after an incubation period in chromium-containing passive alloys and consequently PS tests provide a more conservative estimation of pitting potential than potentiodynamic (PD) tests.[32]

Potentiodynamic- potentiostatic - potentiodynamic (PD-PS-PD) tests were performed to gain further insight into the Low Potential Pitting Corrosion (LPPC) submode of alloys 800 and 690 in 1 M NaCl + 0.001 M $Na_2S_2O_3$ solutions. PD-PS-PD tests consisted of a PD anodic scan that started 50 mV below E_{CORR} and proceeded at a scan rate of 0.0167 mV/s in the noble direction up to a potential in the LPPC zone. At this point, potential was held constant until the circulated charge reached 0.1 C. The potential during the PS stage was set at -110 $mV_{Ag/AgCl}$ for alloy 690 and -160 $mV_{Ag/AgCl}$ for alloy 800. After the PS stage, the potential was scanned in the active direction at a rate of 0.167 mV/s. For these PD-PS-PD tests, a very low potential scan rate (0.0167 mV/s) was used in the forward scan to favor pitting corrosion initiation, while a conventional scan rate (0.167 mV/s) was used in the repassivation scan. When pitting corrosion occurred during the PS stage, the cross-over potential between anodic and cathodic scans was recorded as $E_{RP,LPPC}$.

Potentiostatic tests were performed to study the metastable pitting of alloys 690 and 800 in 1 M NaCl and 1 M NaCl + 0.001 M $Na_2S_2O_3$ solutions. The specimens were masked with an epoxy resin to reduce the submerged area to 0.15 cm^2, in order to decrease the background passive current thus allowing resolution of individual metastable events. OM observations at the end of tests showed that crevice attack did not occur at the epoxy boundary. E_{CORR} was measured for 60 minutes and then the specimens were polarized to 0.2 $V_{Ag/AgCl}$ for 30 minutes. The data acquisition rate during PS tests was set to 30 points/s, which allowed an acceptable characterization of metastable events.

Figure 2 [a] shows a typical metastable event obtained during potentiostatic tests. The metastable events were characterized by an increase in current from background noise current as pits developed and a subsequent sudden decrease of current when a pit repassivated. The metastable pit peak current (I_{peak}) was the difference between the maximum current of the metastable event and the background noise current (Figure 2 [a]). The background noise current in these experiments was on average 8 nA, so only events with I_{peak} 12 nA higher than background noise current were recorded and analyzed. The pit occurrence time (t_{pot}) corresponded to the time when a metastable event reached I_{peak}, as shown in Figure 2 [a]. The time evolution of metastable pit frequency was studied by counting the number of events occurring in time intervals of 100 s, for a total testing time of 1800 s. Some transient overlaps were observed, as shown in Figure 2 [b]. If a current drop was larger than 12 nA, the event was counted as an individual metastable event, otherwise the current drop was considered a partial repassivation followed by the growth of the same metastable pit.[33]

RESULTS AND DISCUSSION

Potentiodynamic behavior in chloride plus thiosulfate solutions

Small additions of thiosulfate to a 1 M NaCl solution had a great impact on the shape of the polarization curve and on its characteristic potentials (E_P, E_{RP}). For a given alloy and solution composition, the measured CPP curve exhibited a shape similar to one of the four reference curves shown in Figure 3 (types A, B, C and D). Experimental conditions and the electrochemical behavior exhibited by each alloy are summarized in Table 3. In pure chloride solutions, all the alloys showed Type A CPP curves (Figure 3 [a]), characterized by the presence of a passive region followed by a pitting potential with a repassivation hysteresis loop, typical of conventional chloride pitting corrosion. Passive current density exhibited values about 10^{-7} A/cm^2, and current transients typical of metastable pitting were observed as potential approached the pitting potential. OM examination revealed localized corrosion damage in all alloys specimens polarized in pure chloride solutions.

Type B CPP curves were observed only in the higher chromium alloy 690 with large additions of thiosulfate, 1 M, Table 3. These curves showed a wide passive region, absence of metastable events and oxygen evolution at high potentials (Figure 3 [b]); thus evidencing pitting inhibition in concentrated thiosulfate solutions, as previously described in literature.[9,11,20] Thiosulfate can act as a pitting inhibitor, probably due to proton consumption by reactions 1 and 2,[1] thus hindering localized acidification necessary to stabilize pits.[15] OM revealed absence of localized corrosion in specimens that exhibited type B behavior, Figure 4 [a].

Type C CPP curves were observed for alloy 600 tested in all the studied chloride plus thiosulfate mixtures, Table 3. Alloys 690 and 800 exhibited this behavior at 0.01 and 0.1 M of $S_2O_3^{2-}$. Unlike Type A electrochemical behavior, Type C curves showed absence of metastable events within the potential range of the hysteresis loop (Figure 3 [c]). Instead, stable pitting was observed at very low potential values, probably due to metastable pit stabilization by $S_2O_3^{2-}$ as proposed by others for alloy 800[12,34] and other chromium bearing alloys.[9,18,35] Pitting damage was observed in alloys 600, 690, and 800 that showed Type C electrochemical behavior. Besides pitting damage, alloy 600 showed also intergranular attack when Type C curves were observed; that is, for all $S_2O_3^{2-}$ studied concentrations, Figure 4 [b]. This figure also shows some remnants of corrosion products with mud crack appearance.

Type D CPP curves were only observed for the higher chromium alloys 690 and 800 in 1 M chloride solutions with dilute $S_2O_3^{2-}$ additions, 0.001 and 0.0005 M, Table 3. The most striking feature of those curves was the anodic current density peak at potentials slightly higher than E_{CORR} (Figure 3 [d]). These curves also showed an E_P and a hysteresis

loop at potentials higher than the potential range of the anodic peak. The anodic current density peak was about 10 μA/cm^2 and was observed in the potential range from -0.14 to -0.05 $V_{Ag/AgCl}$ for alloy 690, and in the range from -0.21 to -0.1 $V_{Ag/AgCl}$ for alloy 800. At higher potentials, both alloys exhibited passive behavior, i.e. current density values about 10^{-7} A/cm^2. Type D curves showed frequent metastable pitting events at potentials within the hysteresis loop potential range, similar to what was observed for Type A curves (pure chloride solutions). E_P and E_{RP} in Type D curves were close to the values measured in pure 1 M NaCl solutions (Type A curves). Pitting damage was observed after Type D curves, similarly to that observed after Types A and C curves. A literature review revealed that anodic current peaks similar to the ones observed in this work appeared in polarization curves run in $Na_2S_2O_3$ containing solutions.[9,22] Tsai et al.[9] reported similar peaks in CPP curves for alloy 690 tested in 0.017 M NaCl at room temperature with $S_2O_3^{2-}$ additions from 0.001 to 0.1, but no information was given about the nature of the associated electrochemical reactions involved. Laycock[22] reported an anodic peak extending from -0.1 to 0.2 $V_{Ag/AgCl}$ for stainless steel 304 and stainless steel 904L (UNS N08904) tested in 1 M NaCl solutions with a concentration of $S_2O_3^{2-}$ ranging from 0.1 to 1 M. The height of this peak increased with $S_2O_3^{2-}$ concentration and with increasing temperature, in the range from 20 to 80°C. This author attributes the peak to re-oxidation of sulfur species previously formed by $S_2O_3^{2-}$ reduction below -0.45 $V_{Ag/AgCl}$. In the present work, the anodic peak observed close to the corrosion potential was associated to a submode of pitting,[24] as will be apparent after considering the rest of the experiments performed.

CPP curves of alloy 600 in chloride plus $S_2O_3^{2-}$ solutions did not show an anodic peak (Figure 5) for any concentration of $S_2O_3^{2-}$ studied. This alloy exhibited stable localized corrosion at potentials where the higher chromium alloys exhibited the anodic peak. The notable feature of this alloy was that the repassivation potential decreased with the decrease in the $S_2O_3^{2-}$ concentration without an apparent threshold. Considering that E_{RP} reached values well below E_{CORR} in deaerated environments, it can be concluded that dilute $S_2O_3^{2-}$ solutions are more aggressive than concentrated solutions for alloy 600, in accord with previous studies.[20]

Figure 6 summarizes E_P, E_{RP} and potential range (width) of the anodic peak obtained from CPP curves of SA+A alloys 600, 690 and 800 in 1 M NaCl solutions with different $S_2O_3^{2-}$ additions. The anodic peak was observed for alloys 690 and 800 when $[S_2O_3^{2-}]$ = 0.001 and 0.0005 M. The upper limit of the potential range of the anodic peaks increased with the increase of $S_2O_3^{2-}$ concentration. On the other hand, the lower limit remained almost constant irrespective of alloy type, heat treatment and solution composition. For alloys 690 and 800, the open triangles (additions of $S_2O_3^{2-}$ of 0.001 M and 0.0005 M to a 1 M NaCl solution) correspond to repassivation potentials of low potential pitting corrosion, as will be explained later in this paper (Figure 13 and explanation in the text). Concentrations of $S_2O_3^{2-}$ of 10^{-3} M and lower caused a minor effect on E_{RP} corresponding to high potential pitting corrosion, Figure 6. For $S_2O_3^{2-}$ concentrations of 0.01 M or larger, a single pitting process was observed, with characteristic potentials that increased with $S_2O_3^{2-}$ concentration, Figure 6.

It is accepted that $S_2O_3^{2-}$ aggressiveness is related to its ability to reduce at pit bottoms, yielding a S_{ads} or sulfide layer, which prevents repassivation. Considering the three major alloy components (Ni, Cr and Fe), S_{ads} has the largest potential range of stability on Ni substrate, being the lowest on Cr substrate.[14] In agreement with this, alloy 600, with the lowest wt. % Cr and the highest wt. % Ni among tested alloys, was the least resistant to pitting corrosion in $Cl^- + S_2O_3^{2-}$ solutions, in the sense that additions of $S_2O_3^{2-}$ as low as 10^{-4} M to a 1 M NaCl solution for alloy 600 caused a decrease in E_{RP} of around 0.6 V with respect to pure 1 M NaCl solutions, Figure 6. Alloy 690 slightly outperformed alloy 800 in the same testing conditions. The modest difference is explained because despite alloy 690 has higher wt. %Cr, it also has higher wt. %Ni than alloy 800, and these elements exhibit the smallest and largest potential ranges of S_{ads} stability in E-pH diagrams[14].

Considering that LPPC requires cooperative action of $S_2O_3^{2-}$ and chloride, it can be considered that LPPC and HPPC merged for all concentrations of $S_2O_3^{2-}$ in alloy 600. The behavior displayed by alloy 690 and 800 in PD tests was quite different to that evidenced for alloy 600, Figure 6. LPPC and HPPC merged at concentrations of $S_2O_3^{2-}$ of 0.01 M or higher for those alloys. For alloys 690 and 800, while a minimum in repassivation potential is apparent at 0.01 M based exclusively on PD results (scatter of full triangles), considering LPPC the minimum in repassivation occurred at a much lower concentration of $S_2O_3^{2-}$, near 0.0005 M. Alloys 690 and 800 exhibited type D behavior at intermediate $S_2O_3^{2-}$ concentrations, Table 3. This behavior can be understood as a threshold condition between the minor effect of $S_2O_3^{2-}$ on E_P and E_{RP} observed in solutions with $[S_2O_3^{2-}]$= 0.0001 M or lower, and the single (merged) pitting process at low potentials, observed at $[S_2O_3^{2-}]$= 0.01 M or higher. At $[S_2O_3^{2-}] \leq 0.0001$ M it is likely that not enough $S_2O_3^{2-}$ was available to be reduced at pit bottoms,[13] hence high potentials are required for stable pit growth and electrochemical behavior is similar to that exhibited in pure chloride solutions.

Potentiostatic (PS) tests in 1 M NaCl vs. 1 M NaCl + 0.001 M $Na_2S_2O_3$

PS tests were performed to further explore LPPC, the pitting process occurring in the potential range where the anodic peak was observed in Type D CPP curves (Figure 3 [d]). PD and PS tests performed in 1 M NaCl and in 1 M NaCl + 0.001 M $Na_2S_2O_3$ on alloy 600 are shown in Figures 7 [a] and [b]. PD tests correspond to the forward anodic polarization step of CPP curves (Figures 3 and 5). For PS tests, the reported current density corresponds to the current density measured at the end of the 20-minute PS step during the 20-minute potentiostatic hold, Figure 7. E_P measured in both PD and PS tests were remarkably low (a decrease of about 0.5 V is apparent in Figure 7) when thiosulfate was added to the chloride solution. In pure chloride solution, metastable events are evident in PD and PS tests, but addition of $S_2O_3^{2-}$ stabilized pitting at lower potentials, hence those events were not observed in PD and PS curves. In most cases, thermal aging had a negative effect on pitting potential values, and it increased the height of the anodic peak, without affecting its position significantly, Figure 7.

For alloy 690, in PS tests at potentials close to those of the anodic peak measured in PD tests in 1 M NaCl + 0.001 M $Na_2S_2O_3$ solution (Type D curve, Figure 3 [d]), the current density increased to values above 30 μA/cm^2. Those current density values were more than an order of magnitude larger than those measured in potentiodynamic tests. As potential kept increasing, eventually current density decreased drastically to values near the passive current density (Figures 7 [c] and [d]). At higher potentials metastable pitting and eventually stable pit growth was observed in both solutions giving place to lower E_P values in the thiosulfate-containing solution compared to those in the pure chloride solution. Results for alloy 800 are similar to those obtained for alloy 690, except for SA+A condition in $S_2O_3^{2-}$ solution where PS and PD curves showed different behaviors (Figures 7 [e] and [f]). In PS curves the current density increased at a potential near -0.2 $V_{Ag/AgCl}$ and afterwards it did not decrease when the specimen was polarized at

higher potentials, Figure 7 [f]. Instead, PD curves showed a Type D behavior (Figure 3 [d]): an anodic peak followed by a passive zone before pitting corrosion occurred. It is likely that pits grew to a larger size in PS vs. PD tests, hence, they did not repassivate upon an increase in potential in SA+A 800 alloy.

Specimens of alloys 690 and 800 in the SA+A condition were polarized for 2 hours at potentials in the range of the corresponding anodic peak: -147 $mV_{Ag/AgCl}$ for alloy 690 and -237 $mV_{Ag/AgCl}$ for alloy 800. Transients shown in Figure 8 suggest an autocatalytic process typical of pitting corrosion. Hemispherically-shaped corrosion pits were observed in both alloys after polarization (Figure 9). S was homogeneously distributed in the pit and at the surrounding areas for alloy 690. Instead, for alloy 800, S was enriched in corrosion products within the pit along with Ni and Cr (Figure 9). S was not detected in the surface surrounding the pit of alloy 800 indicating that its concentration was below the EDS detection limit (0.1 wt. %). Other researchers have observed this type of pits (hemispherically-shaped with corrosion products) on stainless steel 304L (UNS S30403) and alloy 800 tested in chloride plus thiosulfate solutions.[10,17,36] Reported corrosion products were metal sulfides from $S_2O_3^{2-}$ reduction within pits.

Figure 8 combined with the observation of hemispherical pits after potentiostatic polarization at potentials within the anodic peak, Figure 9, suggests that the anodic peak observed in PD curves (Figure 7) can be assigned to a pitting process, occurring at a much lower potential than conventional chloride pitting. In this work, this phenomenon was called LPPC in order to distinguish it from the High Potential Pitting Corrosion (HPPC) observed at potentials about 0.3 $V_{Ag/AgCl}$ (Figures 7 [c], [d], [e] and [f]). Figure 10 shows typical pits of SA alloy 690 formed by HPPC in 1 M NaCl + 0.001 M $Na_2S_2O_3$ and another formed in 1 M NaCl. Conventional chloride pitting in chloride solutions and HPPC in chloride + thiosulfate solutions showed pits with similar morphology, characterized by a lacy cover made up of partially damaged passive film or metal, Figures 10 [a] and [b], respectively. Instead, as mentioned above, LPPC was characterized by uncovered hemispherical pits (Figure 9).

To our knowledge, the LPPC process with repassivation upon an increase in potential has not been previously reported for any other Cr bearing alloy in chloride plus thiosulfate solutions. This behavior is similar to that exhibited by stainless steel 304 in sulfate + thiosulfate solutions.[15] Recently, Zhang et al.[6] reported a non-monotonic increase in current with potential for alloy 600. Those authors[6], working with alloy 600 in 0.1 M NaCl + 5.10^{-5} M $S_2O_3^{2-}$ at 60°C, reported that the rate of current increase after scratching the surface at fixed potential exhibited a maximum at intermediate potentials of -0.12 $V_{Ag/AgCl}$. At a higher potential this rate reduced slightly before increasing again due to chloride pitting corrosion. Probably, the higher Cr content in some of the alloys studied in the present work allowed the repassivation at potentials higher than those corresponding to the anodic peak. It is likely that the threshold chromium content required is near 19.6 wt.%, the amount of chromium in solid solution in alloy 800 (Table 1). When this alloy was aged, and hence the amount of chromium in solid solution decreased, low potential pits did not repassivate when polarized at higher potential (chloride plus thiosulfate solution, Figure 7 [f]).

Figure 11 [a] shows current transients of PS tests for SA+A alloy 800 associated with LPPC and HPPC in 1 M NaCl + 0.001 M $Na_2S_2O_3$. Transient curves of HPPC and conventional chloride pitting showed similar characteristics, that is, an incubation time followed by a steep current density increase. Transient curves of LPPC showed a lower rate of current density increase than HPPC and a negligible incubation time.

Current transients measured during PS tests were fitted with power law functions, linearized according to the following equation:

$$\text{Log}\,(i) = n(t - t_0) + a \qquad (3)$$

where i is the current density, t is the time, t_0 is the incubation time, n is the exponent of the power law function and a is a proportionality constant. Equation 3 was fitted for current density values measured between 1 to 50 μA/cm² in PS tests. For LPPC, the potential was held at -0.11 $V_{Ag/AgCl}$ for alloy 690 and -0.16 $V_{Ag/AgCl}$ for alloy 800. For HPPC and conventional chloride pitting, potential was fixed at 0.3 $V_{Ag/AgCl}$ for both alloys. Figure 11 [b] shows the average and dispersion of n values obtained from three independent experiments. There is more than one order of magnitude of difference between n values fitted to LPPC and HPPC. Independently of the metallurgical condition, alloys 690 and 800 showed slower growth kinetics in LPPC than in HPPC and conventional chloride pitting. HPPC and conventional chloride pitting in all alloys and metallurgical conditions showed similar kinetics of pit growth.

These results suggest that HPPC in 1 M NaCl + 0.001 M $Na_2S_2O_3$ and chloride pitting in 1 M NaCl were essentially the same phenomenon. However, LPPC in 1 M NaCl + 0.001 M $Na_2S_2O_3$ was a different phenomenon which occurred only in a restricted range of potentials and required the addition of $S_2O_3^{2-}$ in certain concentrations to 1 M NaCl. PS tests in pure chloride (1 M NaCl) and pure thiosulfate (0.001 M $Na_2S_2O_3$) solutions at LPPC potentials showed transients curves with current decreasing due to growth of passive films at constant potential (Figure 12). It is evident from Figures 8 and 12 the need of a thiosulfate + chloride synergy to produce LPPC. LPPC only occurred in alloys 690 and 800 for a few of the tested $S_2O_3^{2-}$ concentrations in 1 M NaCl and within a limited potential range which depended on each alloy. The observations reported so far for LPPC can be explained with the mechanism proposed by Newman[13] for pitting corrosion of stainless steels in thiosulfate + sulfate solutions: the restricted range of potentials for thiosulfate-assisted stable pit growth is probably related to the simultaneous need of anodic metal dissolution at incipient pit bottoms and reduction of $S_2O_3^{2-}$ to S_{ads} to prevent repassivation.

Finally, considering that LPPC was a submode of pitting corrosion, it was of interest to explore its repassivation potential by reversing the direction of potential scan once pits grew potentiostatically in the anodic peak potential region. With this objective, PD-PS-PD tests were performed in 1 M NaCl + 0.001 M $Na_2S_2O_3$ for alloys 690 and 800, (Figure 13 [a]).The potential during PS stage was set at the value corresponding to the highest current density within the anodic peak observed in Type D CPP curves (Figure 3 [d]), i.e. -0.11 $V_{Ag/AgCl}$ and -0.16 $V_{Ag/AgCl}$ for alloys 690 and 800, respectively. Pits initiated and grew during the PS stage, and during the reverse potential scan, a hysteresis loop was observed. E_{RP} associated with LPPC ($E_{RP,LPPC}$) were -0.191 $V_{Ag/AgCl}$ and -0.252 $V_{Ag/AgCl}$ for alloys 690 and 800, respectively. Taking $E_{RP,LPPC}$ as a criterion, alloy 800 was slightly more susceptible to be damaged by LPPC than alloy 690 (Figure 13 [b]). E_{CORR} values presented in Figure 13 [b] were measured over a 1 h period. $E_{RP,LPPC}$ values lied close to E_{CORR} for both alloys (Figure 13 [b]) measured in deaerated conditions, making it a more likely mechanism of failure than HPPC, if the required concentration of thiosulfate and chloride are present in the environment.

I. Metaestable pitting in 1 M NaCl and 1 M NaCl+ 0.001 M $Na_2S_2O_3$

In order to elucidate the effect of $S_2O_3^{2-}$ on HPPC observed in alloys 690 and 800 in 1 M NaCl+ 0.001 M $Na_2S_2O_3$ solutions, PS tests at 0.2 $V_{Ag/AgCl}$ in 1 M NaCl and 1 M NaCl + 0.001 M $Na_2S_2O_3$ solutions were

performed. At this potential, within the hysteresis loop of CPP curves (Figure 7) and in the passive region that separated HPPC from LPPC for solutions containing $S_2O_3^{2-}$, the alloys exhibited metastable pitting. Typical current transients obtained for alloys 690 and 800 under both metallurgical conditions in 1 M NaCl and 1 M NaCl + 0.001 M $Na_2S_2O_3$ solutions are shown in Figure 14 [a]. Generally, the metastable pit peak current (I_{peak}) decreased significantly with testing time. At the beginning of the experiment overlapped metastable events were frequent (similar to the one shown in Figure 1 [b]) with I_{peak} values above 10 μA; instead, towards the end of the experiment individual metastable events with I_{peak} lower than 1 μA were common (Figure 14 [b]). The passive layer growth and the decrease in the number of favorable sites for nucleation of new metastable events could have been the cause of the decrease in I_{peak} with testing time.[37]

The metastable pitting frequency (λ) was determined as the number of metastable events per unit time and area in intervals of 100 s (Figure 15). Each data point is the average from three independent experiments. Thiosulfate had a modest effect on λ for both studied alloys. In all cases, λ showed progressive decreasing values with testing time, which is likely related to depletion of favorable sites for metastable pit nucleation and improvement of the properties of the passive layer.[37] The λ values showed higher values at the beginning of tests in the presence of $S_2O_3^{2-}$ when SA+A alloys were used. It is likely that carbides surfaces at grain boundaries of SA+A alloys behave as additional nucleation sites to metastable pits in chloride plus thiosulfate solutions. That effect would occur until the depletion of these sites.

Curves of cumulative distributions of I_{peak} values are shown in Figure 16. Median I_{peak} values were higher in alloy 800 than in alloy 690, and for a given alloy, higher values were measured for the SA+A condition. Figure 16 shows that, when 0.001 M $Na_2S_2O_3$ was added to 1 M NaCl solutions, median I_{peak} values increased for alloys 690 and 800 in both metallurgical conditions. The maximum increase of median I_{peak} values was observed in SA alloy 690; from 10 nA without $S_2O_3^{2-}$ ion to 25 nA in presence of $S_2O_3^{2-}$ ion, that is, an increase of 150%. This increase was modest compared to results shown by other authors. Nakhaie et al.,[38] studying UNS S31600 reported that when 0.01 M $S_2O_3^{2-}$ was added to 1 M NaCl solutions, I_{peak} increased from 19 nA to 482 nA, i.e.an increase of 2536%. Wang et al.[39]showed that in stainless steel 304L, I_{peak} increased a 465% (80 nA to 372 nA) when 0.0018 M $S_2O_3^{2-}$ was added to 0.6 M NaCl solutions. In the present work, $S_2O_3^{2-}$ had a modest effect on metastable pitting, characterized during potentiostatic scans at 0.2 $V_{Ag/AgCl}$. This value is close to the threshold upper potential required for sulfur adsorption at pit bottoms.[14] The modest effect of $S_2O_3^{2-}$ at high potentials is in contrast with the catastrophic effect when added to a chloride solution at a low potential, shown in Figure 12 vs. Figure 8.

II. Summary of electrochemical behavior in 1 M NaCl and 1 M NaCl + 0.001 M $Na_2S_2O_3$

Figure 17 summarizes the effect of potential on the electrochemical behavior of the three studied alloys, as obtained from PS polarization tests in 1 M NaCl and 1 M NaCl + 0.001 M $Na_2S_2O_3$ (Figure 7). Occurrence of LPPC reduced significantly the zone of stable passivity for alloys 690 and 800, especially when the alloy was in the SA+A condition. In 1 M NaCl + 0.001 M $Na_2S_2O_3$, SA alloy 800 outperformed SA alloy 690. However, for alloy 800 in the SA+A condition, low potential corrosion pits did not repassivate at noble potentials, and this pitting process merged with chloride pitting or HPPC. In alloy 600, due its lower chromium content, thiosulfate pitting merged with chloride pitting as potential increased, in accord with previous studies.[6,13]

Conclusions

Pitting corrosion of 600, 800 and 690 alloys was studied in 1 M chloride solutions with different concentrations of $S_2O_3^{2-}$, the main findings are summarized below:

- Alloy 600 exhibited a single pitting mode, with pitting and repassivation potentials that decreased with decreasing $S_2O_3^{2-}$ concentration. A detrimental effect of $S_2O_3^{2-}$ on stable pitting and repassivation potentials were measured for [$S_2O_3^{2-}$] as low as 10^{-4} M.

- For alloys 690 and 800, a single pitting process was observed for [$S_2O_3^{2-}$] of 0.01 M or larger. Under such conditions, these alloys exhibited pitting at very low potentials that merged with chloride pitting as potential was increased, hence a monotonic i vs. E curve was observed in potentiodynamic tests. Pitting and repassivation potentials increased with increasing thiosulfate content, in the range of 0.01 to 1 M.

- When $S_2O_3^{2-}$ concentration was 1 M, complete inhibition of pitting corrosion was observed in alloy 690. It is likely that, when $S_2O_3^{2-}$ dominates in the environment, it has an inhibiting effect because its reduction and disproportionation reaction consumes protons hindering localized acidification required for stable pit growth.

- Two different submodes of pitting corrosion were clearly distinguished in alloys 690 and 800 tested in 1 M NaCl + 0.001 M $Na_2S_2O_3$. High potential pitting corrosion exhibited lacy covered pits that grew with a similar kinetics compared with that observed in pure chloride solutions. This pitting submode was characterized by frequent metastable pitting at lower potential, long incubation times and very rapid growth rate. Low potential pitting corrosion exhibited hemispherical pits with a slower growth kinetic, with essentially no incubation time at this concentration of chloride.

- Low potential pits, observed in 1 M NaCl + 0.001 M $Na_2S_2O_3$ solution, can repassivate if potential is scanned either in the active or noble direction.

- Low potential pitting corrosion could be a concern for materials in industrial plants because it can occur even at potentials close to the corrosion potential in deaerated solutions.

- In general, pitting corrosion susceptibility of aged alloys was higher than that of fully solubilized alloys. Higher metastable pitting transient rate and maximum current of metastable events were observed for aged alloys, which could have been related to the increase in number of nucleation sites, like precipitated carbides at grain boundaries.

- At a sufficiently high electrochemical potential, $S_2O_3^{2-}$ had a modest effect on metastable pitting, probably because it could not reduce at pit bottoms.

References

1. L. Choudhary, D. D. Macdonald, A. Alfantazi, *Corrosion* 71 (2015): p. 1147–1168.
2. A. Garner, *Corrosion* 41 (1985): p. 587-591.
3. A. M. Brennenstuhl, T. S. Gendron, R. Cleland, *Corrosion Science* 35 (1993): p. 699-711.
4. R. W. Staehle, J. A. Gorman, *Corrosion* 60 (2004): p. 115-180.
5. R. Roberge, *Corrosion* 44 (1988): p. 274-280.
6. W. Zhang, A. G. Carcea, R. C. Newman, *Faraday Discuss* 180 (2015): p. 233-249.

7. J. T. Ho, G. P. Yu, *Corrosion* 48 (1992): p. 147-158.
8. I. J. Yang, *Corrosion Science* 49 (1993): p. 576-584.
9. W. T. Tsai, T. F. Wu, *Journal of Nuclear Materials* 277 (2000): p. 169-174.
10. D. Xia, S. Song, R. Zhu, Y. Behnamian, C. Shen, J. Wang, J. Luo, Y. Lu, S. Klimas, *Electrochimica Acta* 111 (2013): p. 510-525.
11. D. Xia, H. Fan, L. Yang, Y. Behnamian, J. Luo, Y. Lu, S. Klimas, *Journal of The Electrochemical Society* 162 (2015): p. C482-C486.
12. D. Xia, R. Zhu, Y. Behnamian, J. Luo, Y. Lu, C. Lin, S. Klimas, *Journal of Electroanalytical Chemistry* 744 (2015): p. 77–84.
13. R. C. Newman, W. P. Wong, H. Ezuber, A. Garner, *Corrosion* 45 (1989): p. 282–287.
14. P. Marcus, E. Protopopoff, *Corrosion Science* 39 (1997): p. 1741-1752.
15. R. C. Newman, *Corrosion* 41 (1985): p. 450-453.
16. P. Marcus, *Journal of The Electrochemical Society* 137 (1990): p. 2709- 2712.
17. R.C. Newman, H.S. Isaacs, B. Alman, *Corrosion* 38 (1982): p. 261–265.
18. C. Duret-Thual, D. Costa, W.P. Yang, P. Marcus, *Corrosion Science* 39 (1997): p. 913–933.
19. M. Naghizadeh, D. Nakhaie, M. Zakeri, M.H. Moayed, *Journal of The Electrochemical Society* 162 (2015): p. C71–C77
20. M. Y. Chang, G. P. Yu, *Journal of Nuclear Materials* 202 (1993): p. 145-153.
21. J. J. Park, S. I. Pyun, *Corrosion Science* 46 (2004): p. 285-296.
22. N. J. Laycock, *Corrosion* 55 (1999): p. 590–595.
23. R. W. Staehle, *Corrosion* 55 (1999): p. 355–379.
24. A. A. Becerra, M. A. Rodríguez, M. A. Kappes, R. B. Rebak, R. M. Carranza, "Effect of Thiosulfate on the Pitting Corrosion of Nickel Base Alloys in Chloride Solutions," Proceedings of Corrosion/2017, paper no. 9036 (New Orleans, LA: NACE, 2017).
25. "Lifetime prediction of materials in environments" R. W. Staehle, Uhlig's Corrosion Handbook, Third Edition, Edited by R. Winston Review Copyright 2011 John Wiley & Sons, Inc.
26. D. A. Jones, Principles and prevention of corrosion, Second Edition, Edited by Pearson Education.
27. M. G. Fontana, Corrosion Engineering, Third Edition, 1986 McGraw-Hill Book Company.
28. R. W. Staehle, J. A. Gorman, *Corrosion* 59 (2003): p. 931–994.
29. M. E. Gonzalez, M. A. Kappes, M. A. Rodríguez, P. Bozzano, R. M. Carranza, R. B. Rebak, *Corrosion* 74 (2018): p. 210-224.
30. R. E. Gold, D.L. Harrod, R.G. Aspden, A.J. Baum, "Alloy 690 for Steam Generator Tubing Applications," EPRI NP-6997-SD Electric Power Research Institute (1990).
31. D. L. Harrod, R. E. Gold, R. J. Jacko, *The Journal of The Minerals, Metals & Materials Society* 53 (2001): p. 14–17.
32. J. R. Galvele, J. B. Lumsden, R. W. Staehle, *Journal of The Electrochemical Society* 125 (1978): p. 1204–1208.
33. N. J. Laycock, R. C. Newman, *Corrosion Science* 39 (1997): p. 1771–1790.
34. S. Wu, J. Wang, S. Song, D. Xia, Z. Zhang, Z. Gao, J. Wang, W. Jin, W. Hu, *Journal of The Electrochemical Society*. 164 (2017): p. C94–C103
35. D. E. Williams, C. Westcott, M. Fleischmann, *Journal of The Electrochemical Society* 132 (1985): p. 1796–1804.
36. T. Laitinen, Corrosion Science 42 (2000): p. 421–441.
37. L. Stockert, H. Böhni, *Materials Science Forum* 44–45 (1989): p. 313–328.
38. M. Naghizadeh, D. Nakhaie, M. Zakeri, M.H. Moayed, *Journal of The Electrochemical Society* 162 (2015): p. C121–c127
39. Y. Wang, G. Wu, L. He, P. M. Singh, *Corrosion* 72 (2016): p. 628–635.

FIGURE CAPTIONS

FIGURE 1: SEM images of grain boundaries after: a, b, c) SA treatment, and d, e, f) SA+A treatment.

FIGURE 2. Types of metastable events developed on alloys 690 and 800 at 0.2 $V_{Ag/AgCl}$ in 1 M NaCl and 1 M NaCl + 0.001 M $Na_2S_2O_3$ solutions: a) single event, and b) overlapped events. Key characteristics of metastable events are graphically presented in a).Results correspond to SA alloy 690.

FIGURE 3. Examples of different behaviors exhibited during CPP tests in thiosulfate and chloride solutions: Type A (1 M NaCl), Type B (1 M NaCl + 1 M $Na_2S_2O_3$), Type C (1 M NaCl + 0.01 M $Na_2S_2O_3$) and Type D (1 M NaCl + 0.001 M $Na_2S_2O_3$). Results correspond to SA+A alloy 690.

FIGURE 4. Optical micrographs observed after CPP tests showing: a) absence of localized corrosion in 1 M NaCl + 1 M $Na_2S_2O_3$ on SA+A alloy 690 and b) intergranular attack in 1 M NaCl + 0.001 M $Na_2S_2O_3$ on SA+A alloy 600.

FIGURE 5. CPP curves in 1 M NaCl solution plus $Na_2S_2O_3$ additions for SA+A alloy 600.

FIGURE 6. Effect of $S_2O_3^{2-}$ concentration on E_P and E_{RP} potentials and position and width of the anodic peak, for CPP and PD-PS-PD tests conducted in 1 M NaCl base electrolyte.

FIGURE 7. PD and PS polarization curves in 1 M NaCl with and without 0.001 M $Na_2S_2O_3$ for a) SA alloy 600, b) SA+A alloy 600, c) SA alloy 690, d) SA+A alloy 690, e) SA alloy 800 and f) SA+A alloy 800. Arrows in PS curves indicate i >30 μA/cm².

FIGURE 8. Currents transients developed during PS test at a potential within the anodic peak of Figure 2 (type D), performed in 1 M NaCl + 0.001 M $Na_2S_2O_3$ for: SA+A alloy 690 at -147 $mV_{Ag/AgCl}$ and SA+A alloy 800 at -237 $mV_{Ag/AgCl}$.

FIGURE 9. SEM images and EDS maps of S, Cr, Ni and Fe in a low potential pit formed in 1 M NaCl + 0.001 M $Na_2S_2O_3$ on a) SA+A alloy 690at -147 $mV_{Ag/AgCl}$ and b) SA+A alloy 800 at -237 $mV_{Ag/AgCl}$.

FIGURE 10. Micrographs of high potential pits observed on SA alloy 690 after PS test in: a) 1 M NaCl and b) 1 M NaCl + 0.001 M $Na_2S_2O_3$, polarized at 0.3 $V_{Ag/AgCl}$.

FIGURE 11. a) Typical currents transients developed during PS test at breakdown potentials associated with LPPC and HPPC in 1 M NaCl + 0.001 M $Na_2S_2O_3$. Results shown for SA+A alloy 800. b) Exponent n of the power law function for stable pit growth during PS tests at potentials associated with LPPC and HPPC in 1 M NaCl + 0.001 M $Na_2S_2O_3$, and pure chloride pitting in 1 M NaCl.

FIGURE 12. Typical currents transients developed during PS test at potential of LPPC in pure chloride and pure thiosulfate solutions. Results shown for SA Alloy 690.

FIGURE 13. a) Typical i vs. E response of SA+A alloy 690 recorded during PD-PS-PD tests, and b) $E_{RP,LPPC}$ values for alloys 690 and 800 measured by PD-PS-PD tests in deaerated conditions.

FIGURE 14. a) Typical current transients developed during PS test at 0.2 $VAg_{/AgCl}$ for SA+A alloy 800. b) Magnified interval time of current transients observed in a).

FIGURE 15. Metastable pitting occurrence frequency during PS tests at 0.2 $V_{Ag/AgCl}$ for: a) SA alloy 690, b) SA+A alloy 690, c) SA alloy 800 and d) SA+A alloy 800.

FIGURE 16. Cumulative probability of metastable pit peak current obtained from PS tests at 0.2 $V_{Ag/AgCl}$ for: a) alloy 690 and b) alloy 800.

FIGURE 17. Potential ranges associated with passivity and pitting corrosion for tested alloys in 1 M NaCl and 1 M NaCl + 0.001 M $Na_2S_2O_3$.

Tables

Table 1
Chemical composition of the tested alloys in weight percent

Alloy	Ni	Cr	Fe	C	Mn	Si	Ti
600	75.8	14.1	8.64	0.150	0.200	0.220	0.260
690	60.3	29.8	9.90	0.0272	0.0210	0.254	0.0374
800	30.5	19.6	45.6	0.100	0.650	0.330	0.640

Table 2
Heat treatments performed to the tested alloys

Heat Treatment	Temperature	Time	Cooling
Solubilization Annealing (SA)	1100 ºC	25 minutes	Water
Aging (A)	716 ºC	10 hours	Air

Table 3
Summary of electrochemical behaviors observed under different studied conditions, with reference to Figure 3.

[NaCl], (M)	$[S_2O_3^{2-}]$, (M)	Type of curve					
		Alloy 600		Alloy 690		Alloy 800	
		SA	SA+A	SA	SA+A	SA	SA+A
1	0	A	A	A	A	A	A
1	0.0001	C	C	A	A	A	A
1	0.0005	C	C	A	D	D	D
1	0.001	C	C	D	D	D	D
1	0.01	C	C	C	C	C	C
1	0.1	C	C	C	C	C	C
1	1	C	C	B	B	C	C

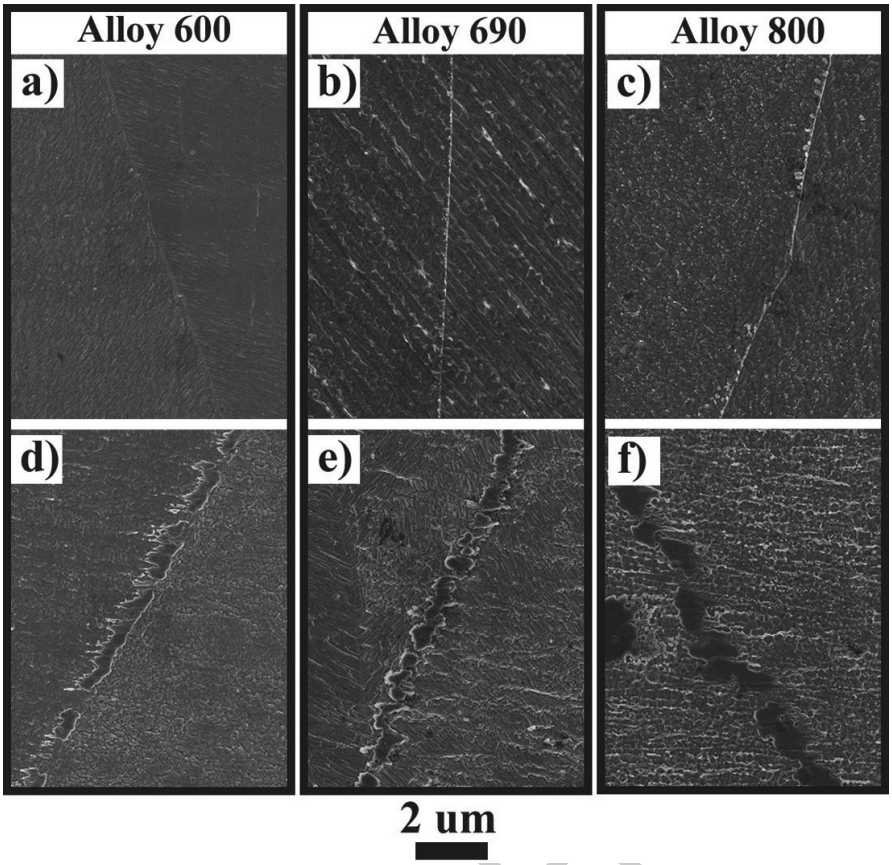

FIGURE 1: SEM images of grain boundaries after: a, b, c) SA treatment, and d, e, f) SA+A treatment.

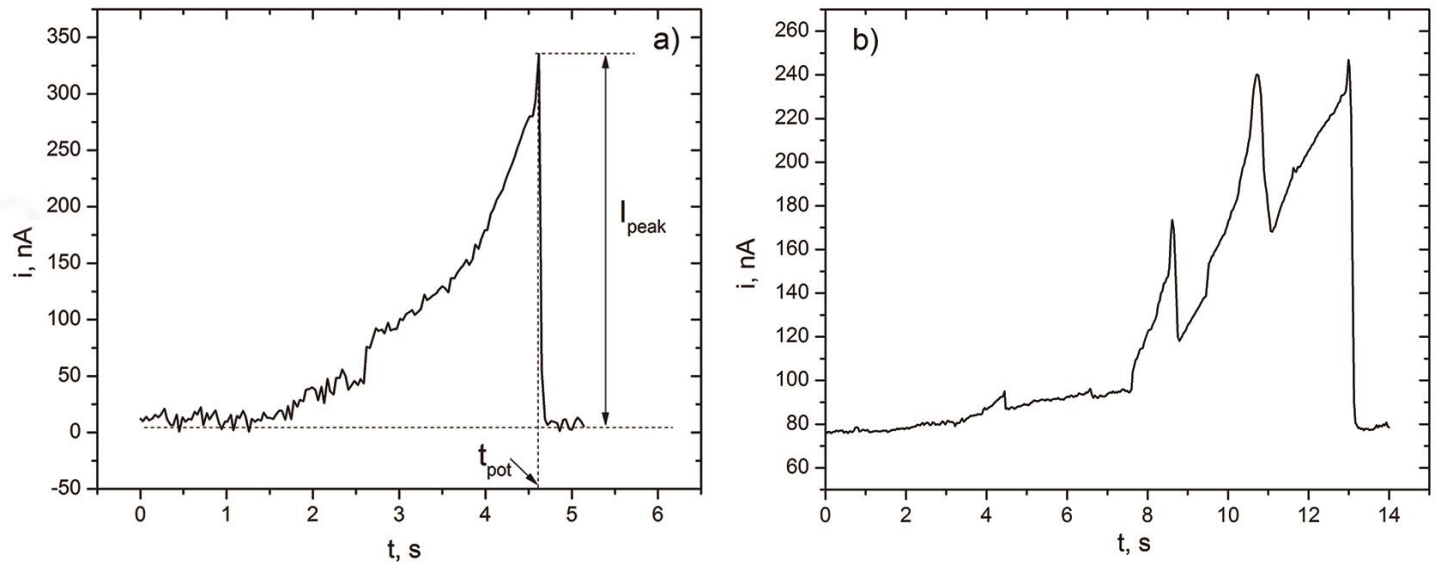

FIGURE 2.Types of metastable events developed on alloys 690 and 800 at 0.2 $V_{Ag/AgCl}$ in 1 M NaCl and 1 M NaCl + 0.001 M $Na_2S_2O_3$ solutions: a) single event, and b) overlapped events. Key characteristics of metastable events are graphically presented in a). Results correspond to SA alloy 690.

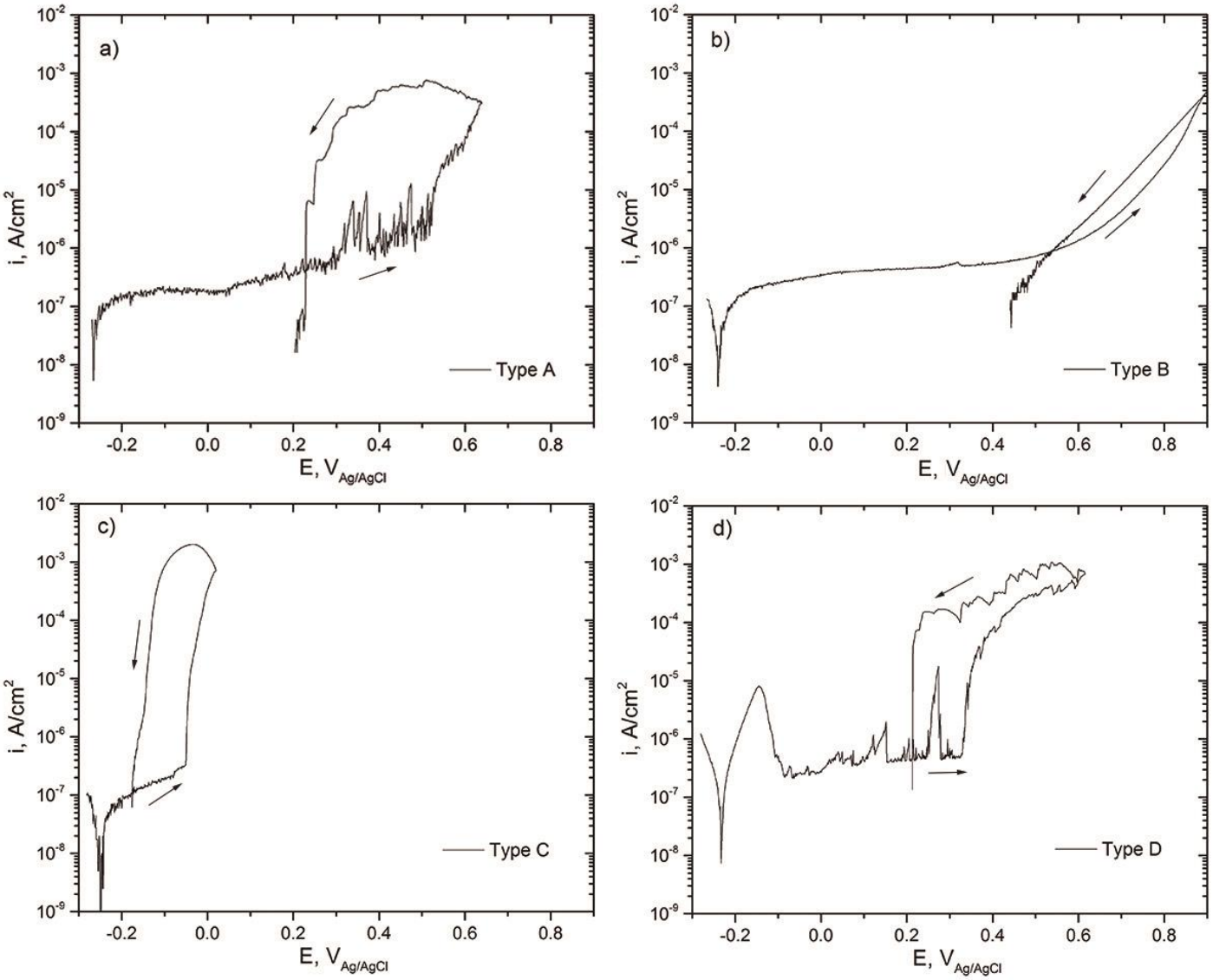

FIGURE 3.Examples of different behaviors exhibited during CPP tests in thiosulfate and chloride solutions: a) Type A: 1 M NaCl, b) Type B: 1 M NaCl + 1 M $Na_2S_2O_3$, c) Type C: 1 M NaCl + 0.01 M $Na_2S_2O_3$ and d) Type D: 1 M NaCl + 0.001 M $Na_2S_2O_3$. Results correspond to SA+A alloy 690.

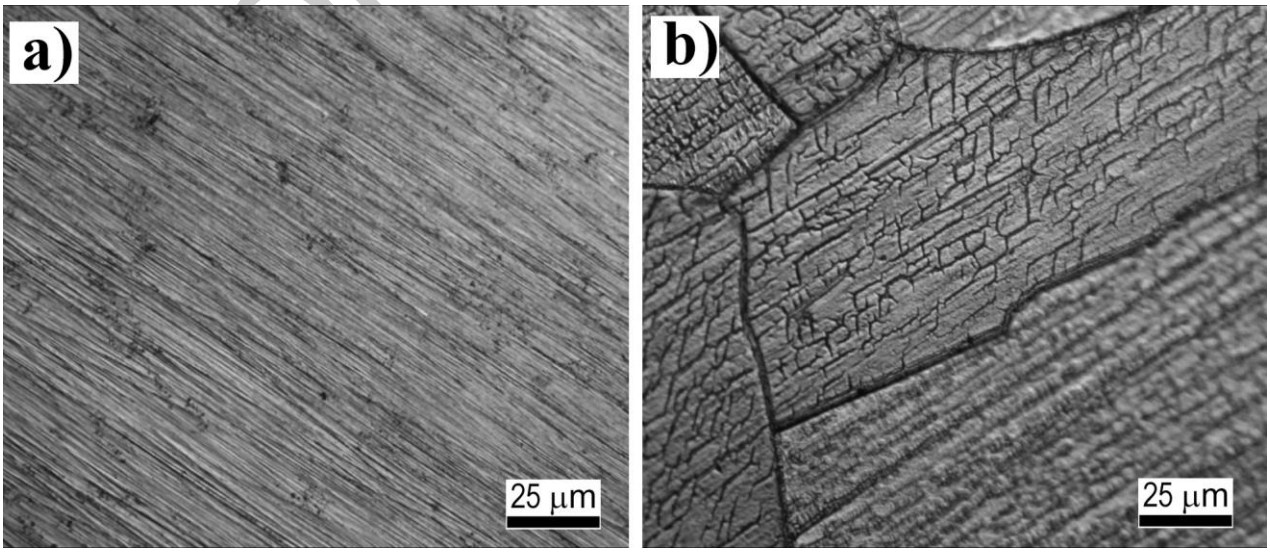

FIGURE 4.Optical micrographs observed after CPP tests showing: a) absence of localized corrosion in 1 M NaCl + 1 M $Na_2S_2O_3$ on SA+A alloy 690 and b) intergranular attack in 1 M NaCl + 0.001 M $Na_2S_2O_3$ on SA+A alloy 600.

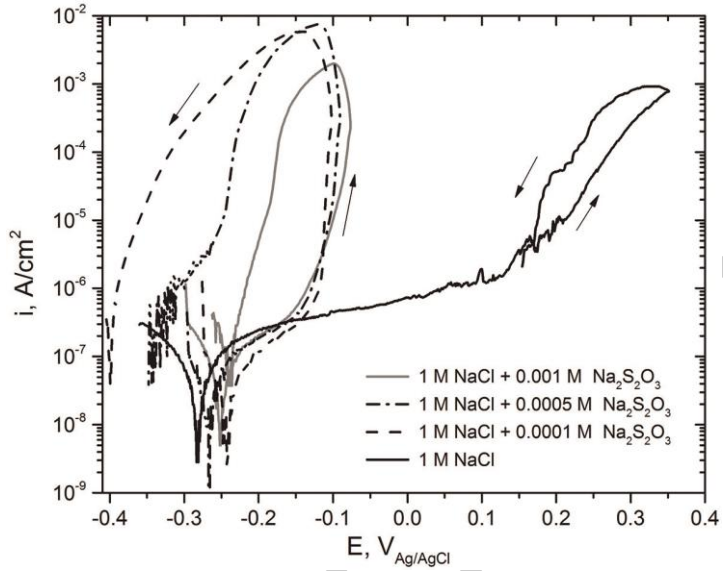

FIGURE 5.CPP curves in 1 M NaCl solution plus $Na_2S_2O_3$ additions for SA+A alloy 600.

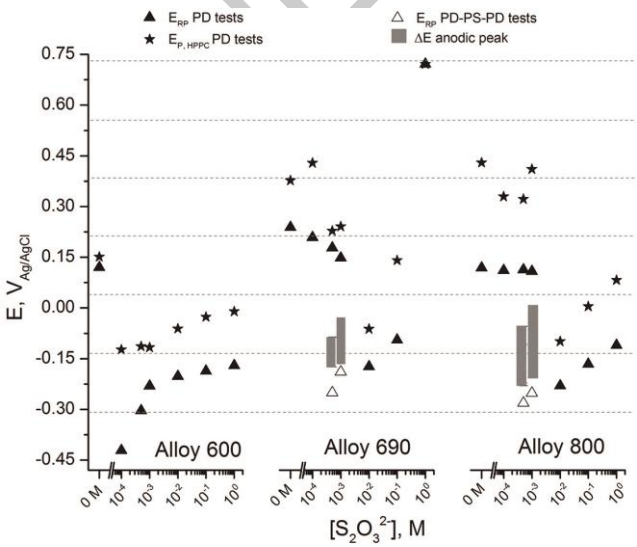

FIGURE 6.Effect of $S_2O_3^{2-}$ concentration on E_P and E_{RP} potentials and position and width of the anodic peak, for CPP and PD-PS-PD tests conducted in 1 M NaCl base electrolyte. Alloys tested in the SA+A condition.

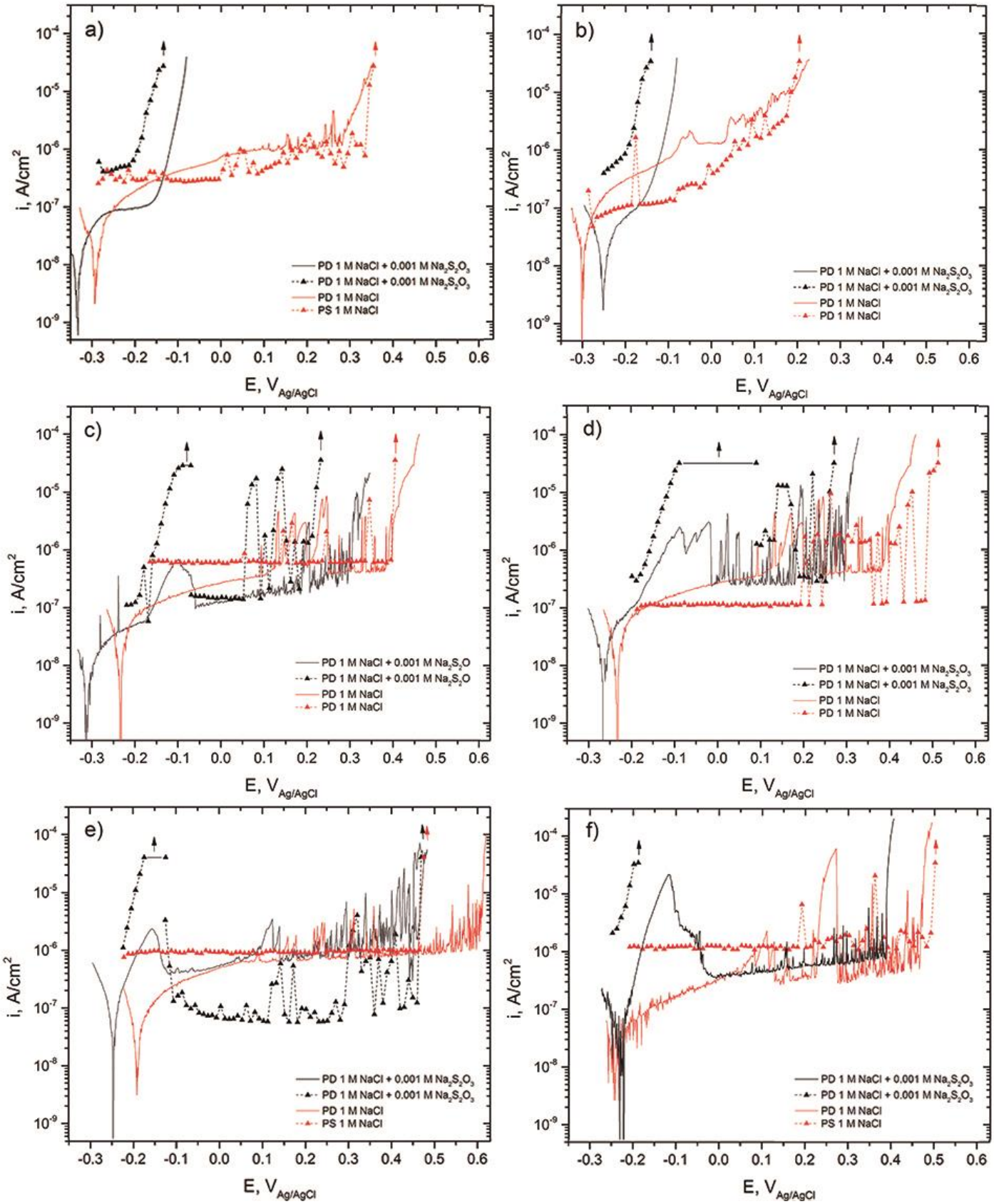

FIGURE 7. PD and PS polarization curves in 1 M NaCl with and without 0.001 M $Na_2S_2O_3$ for a) SA alloy 600, b) SA+A alloy 600, c) SA alloy 690, d) SA+A alloy 690, e) SA alloy 800 and f) SA+A alloy 800. Arrows in PS curves indicate i >30 μA/cm².

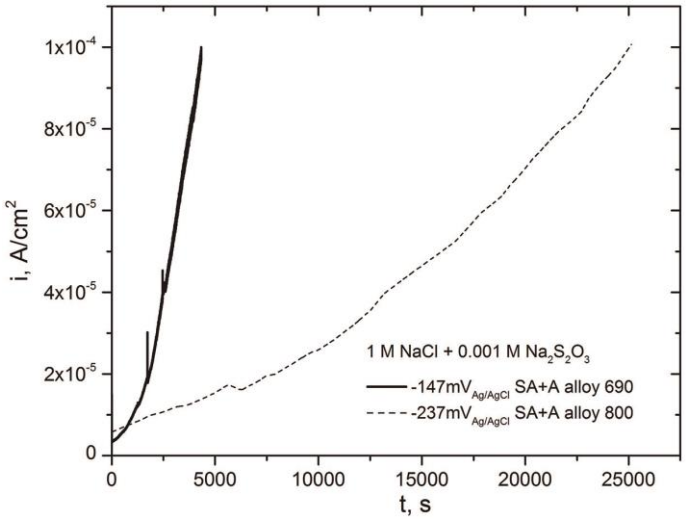

FIGURE 8.Currents transients developed during PS test at a potential within the anodic peak of Figure 2 (type D), performed in 1 M NaCl + 0.001 M $Na_2S_2O_3$ for: SA+A alloy 690 at -147 $mV_{Ag/AgCl}$ and SA+A alloy 800 at -237 $mV_{Ag/AgCl}$.

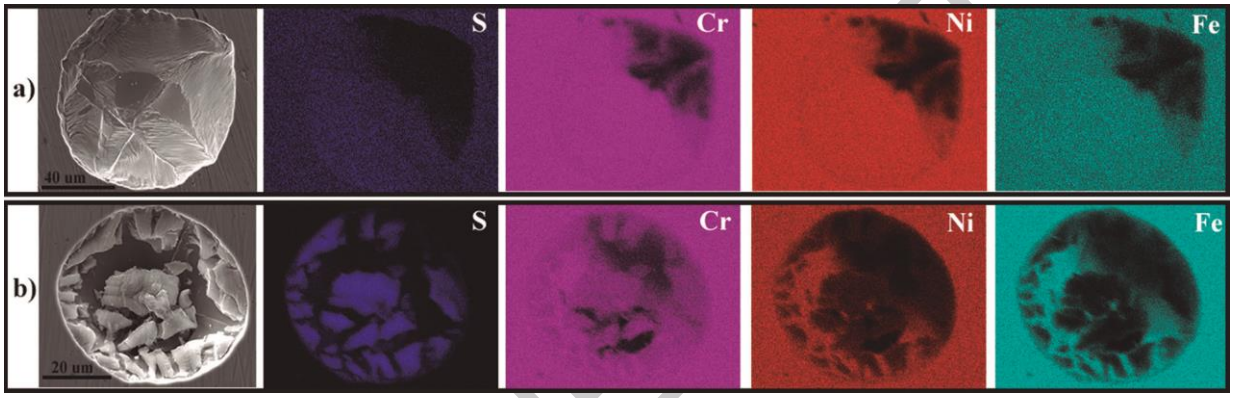

FIGURE 9.SEM images and EDS maps of S, Cr, Ni and Fe in a low potential pit formed in 1 M NaCl + 0.001 M $Na_2S_2O_3$ on a) SA+A alloy 690 at -147 $mV_{Ag/AgCl}$ and b) SA+A alloy 800 at -237 $mV_{Ag/AgCl}$.

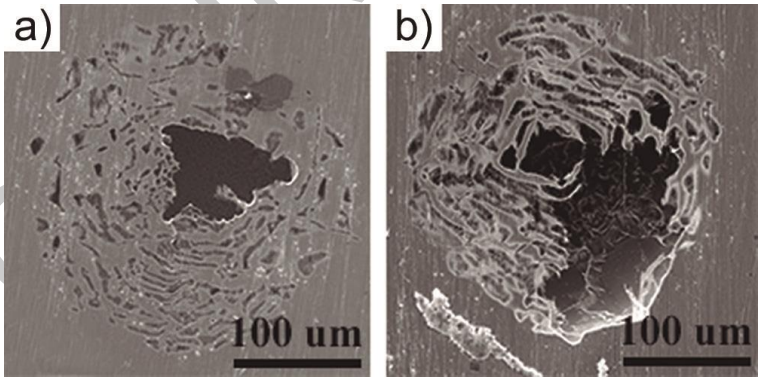

FIGURE 10.Micrographs of high potential pits observed on SA alloy 690 after PS test in: a) 1 M NaCl and b) 1 M NaCl + 0.001 M $Na_2S_2O_3$, polarized at 0.3 $V_{Ag/AgCl}$.

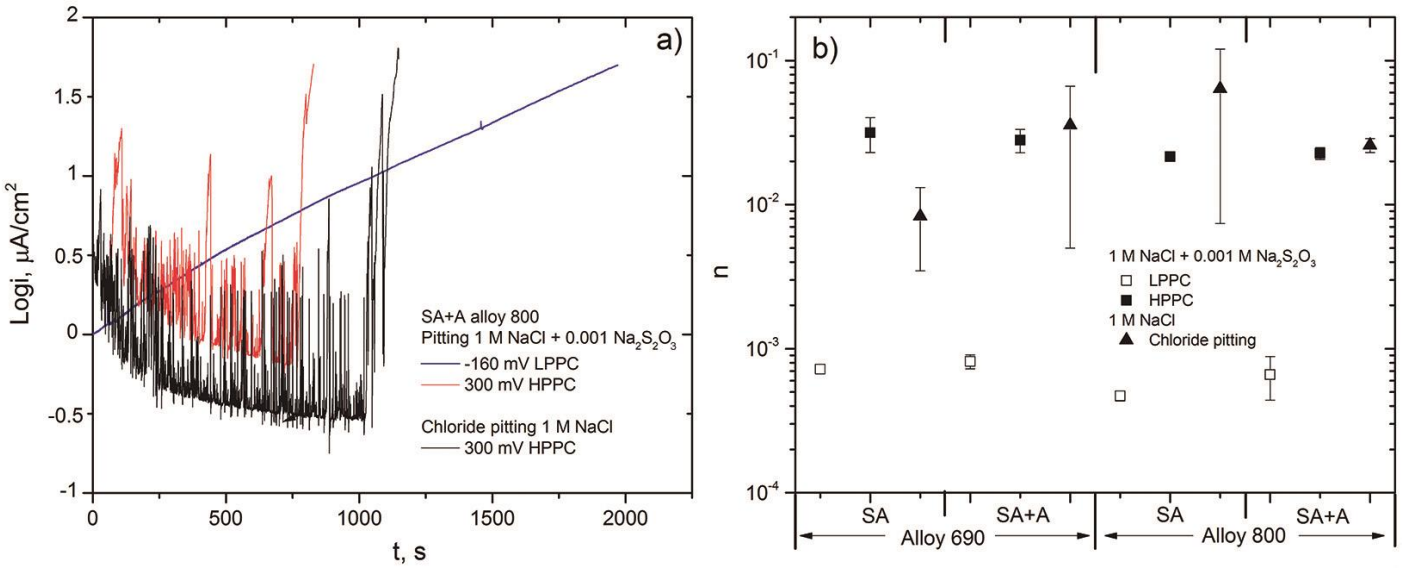

FIGURE 11.a) Typical currents transients developed during PS test at breakdown potentials associated with LPPC and HPPC in 1 M NaCl + 0.001 M $Na_2S_2O_3$. Results shown for SA+A alloy 800. b) Exponent *n* of the power law function for stable pit growth during PS tests at potentials associated with LPPC and HPPC in 1 M NaCl + 0.001 M $Na_2S_2O_3$, and pure chloride pitting in 1 M NaCl.

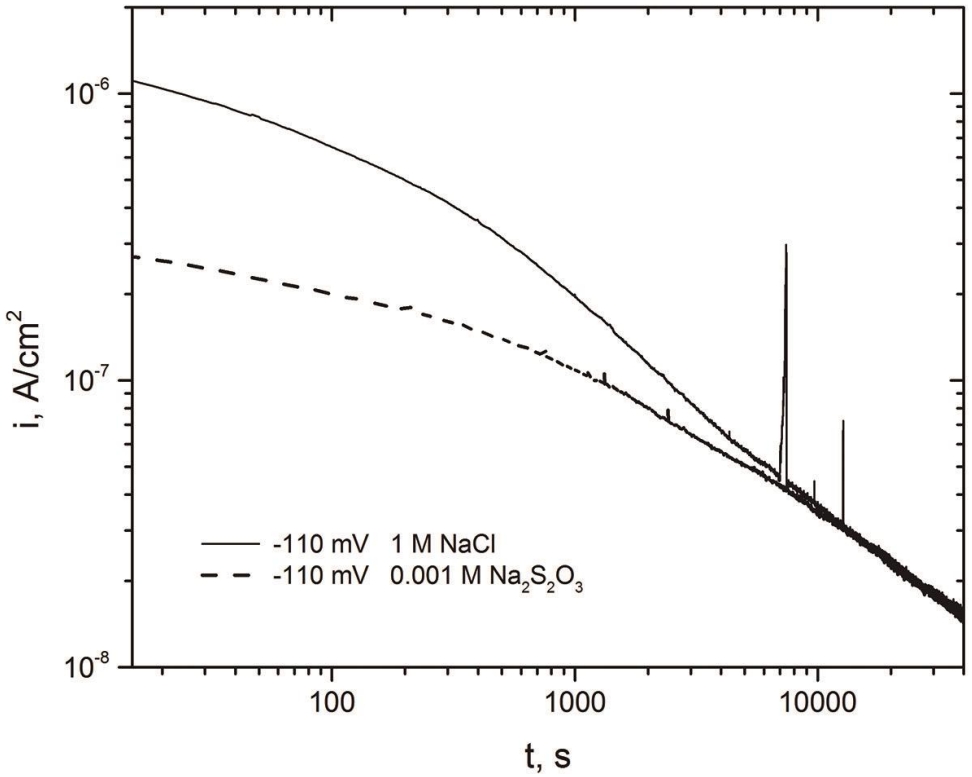

FIGURE 12.Typical currents transients developed during PS test at potential of LPPC in pure chloride and pure thiosulfate solutions. Results shown for SA alloy 690.

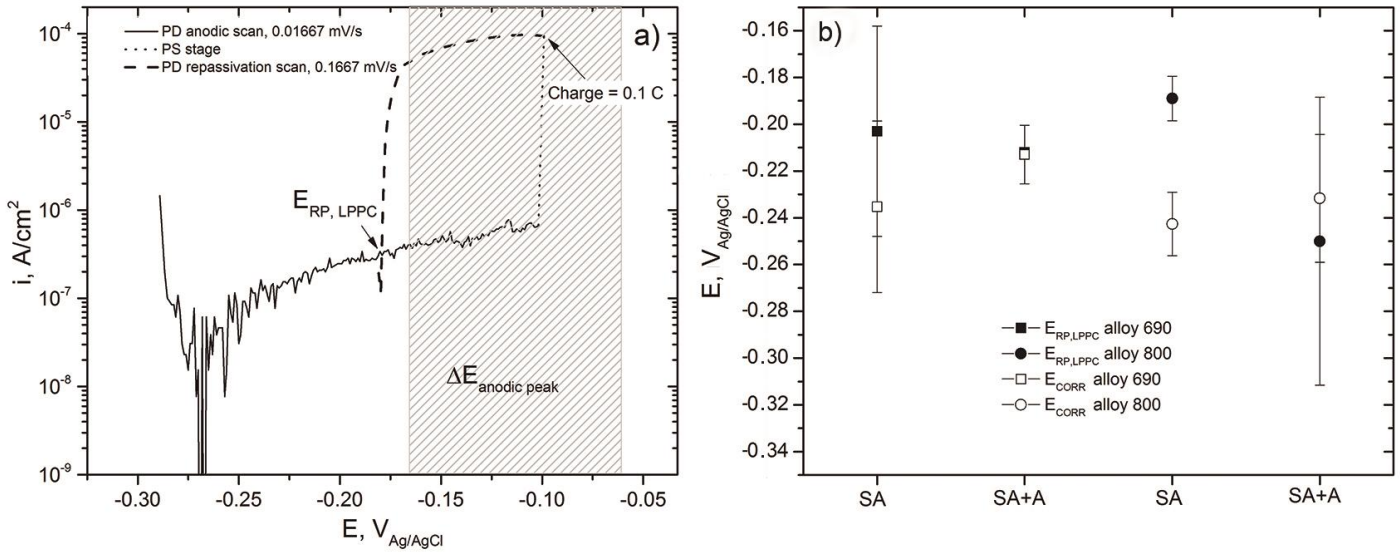

FIGURE 13.a) Typical i vs. E response of SA+A alloy 690 recorded during PD-PS-PD tests, and b) $E_{RP,LPPC}$ values for alloys 690 and 800 measured by PD-PS-PD tests in deaerated conditions. Results obtained in solution 1 M NaCl + 0.001 M $Na_2S_2O_3$.

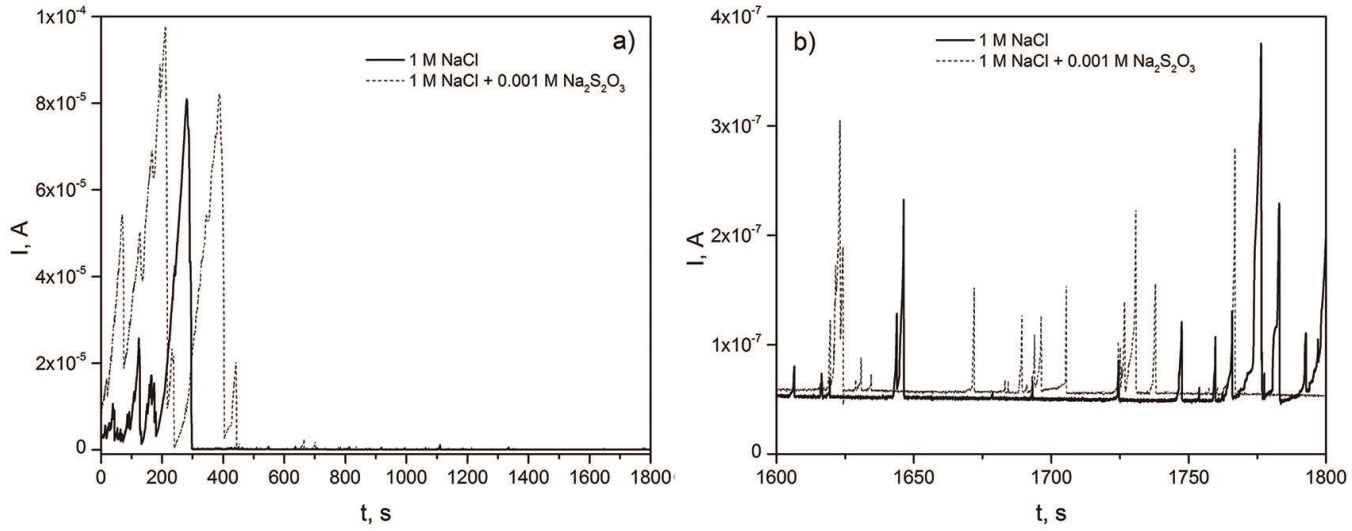

FIGURE 14.a) Typical current transients developed during PS test at 0.2 $V_{Ag/AgCl}$ for SA+A alloy 800. b) Magnified interval time of current transients observed in a).

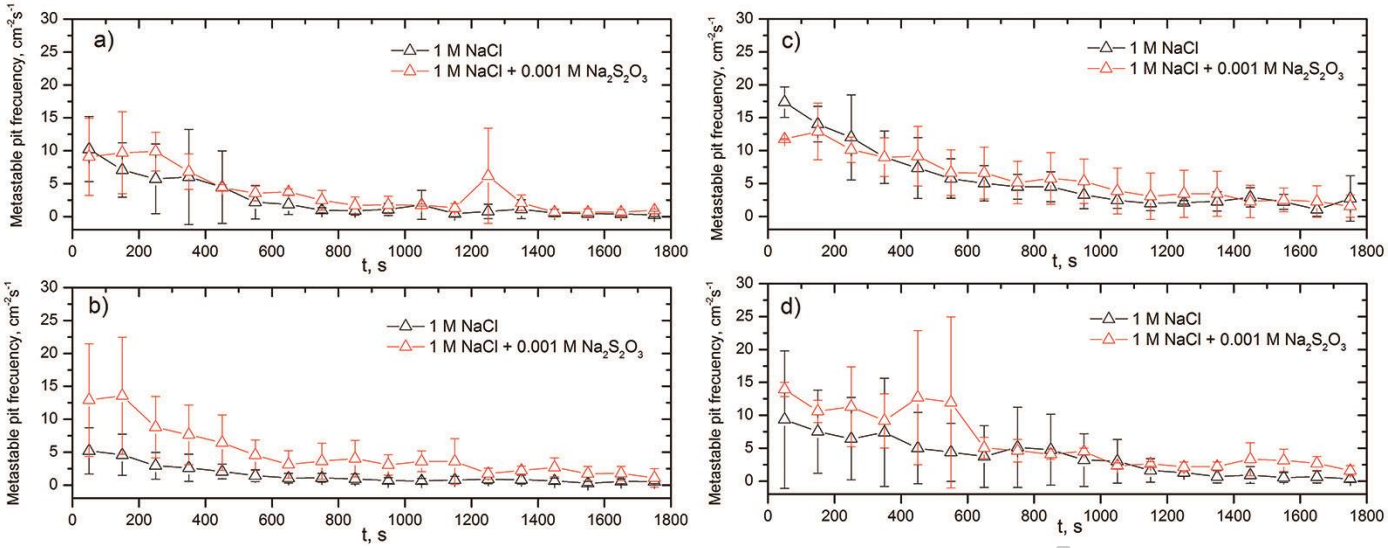

FIGURE 15.Metastable pitting occurrence frequency during PS tests at 0.2 $V_{Ag/AgCl}$ for: a) SA alloy 690, b) SA+A alloy 690, c) SA alloy 800 and d) SA+A alloy 800.

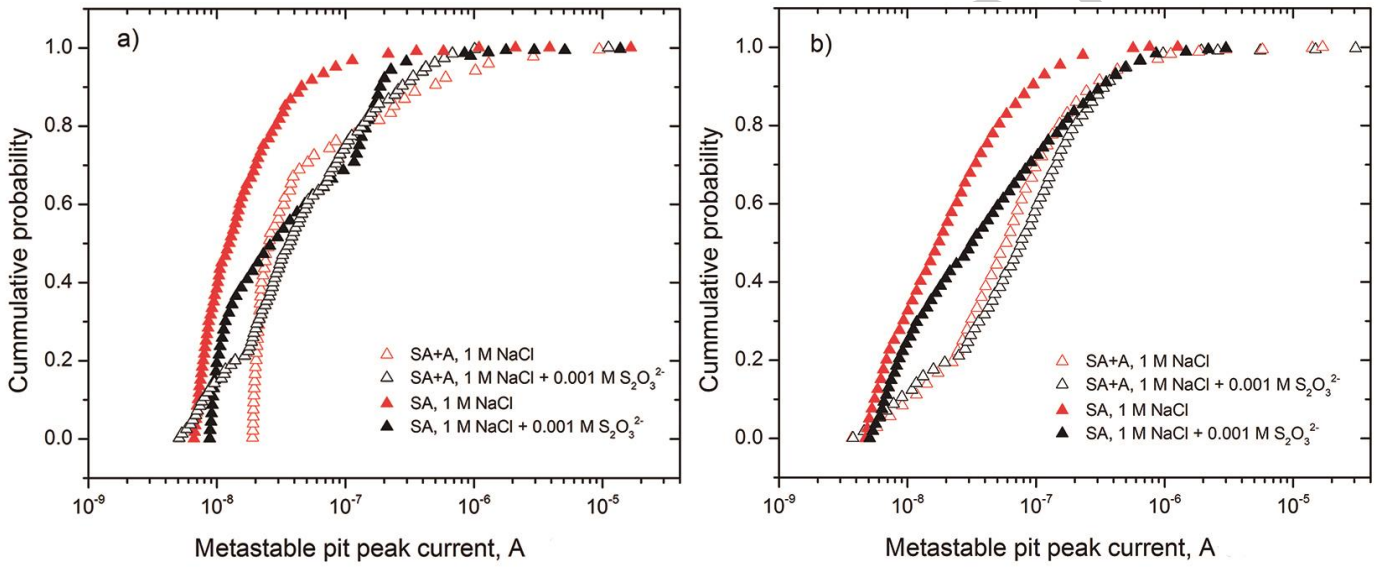

FIGURE 16.Cumulative probability of metastable pit peak current obtained from PS tests at 0.2 $V_{Ag/AgCl}$ for: a) alloy 690 and b) alloy 800.

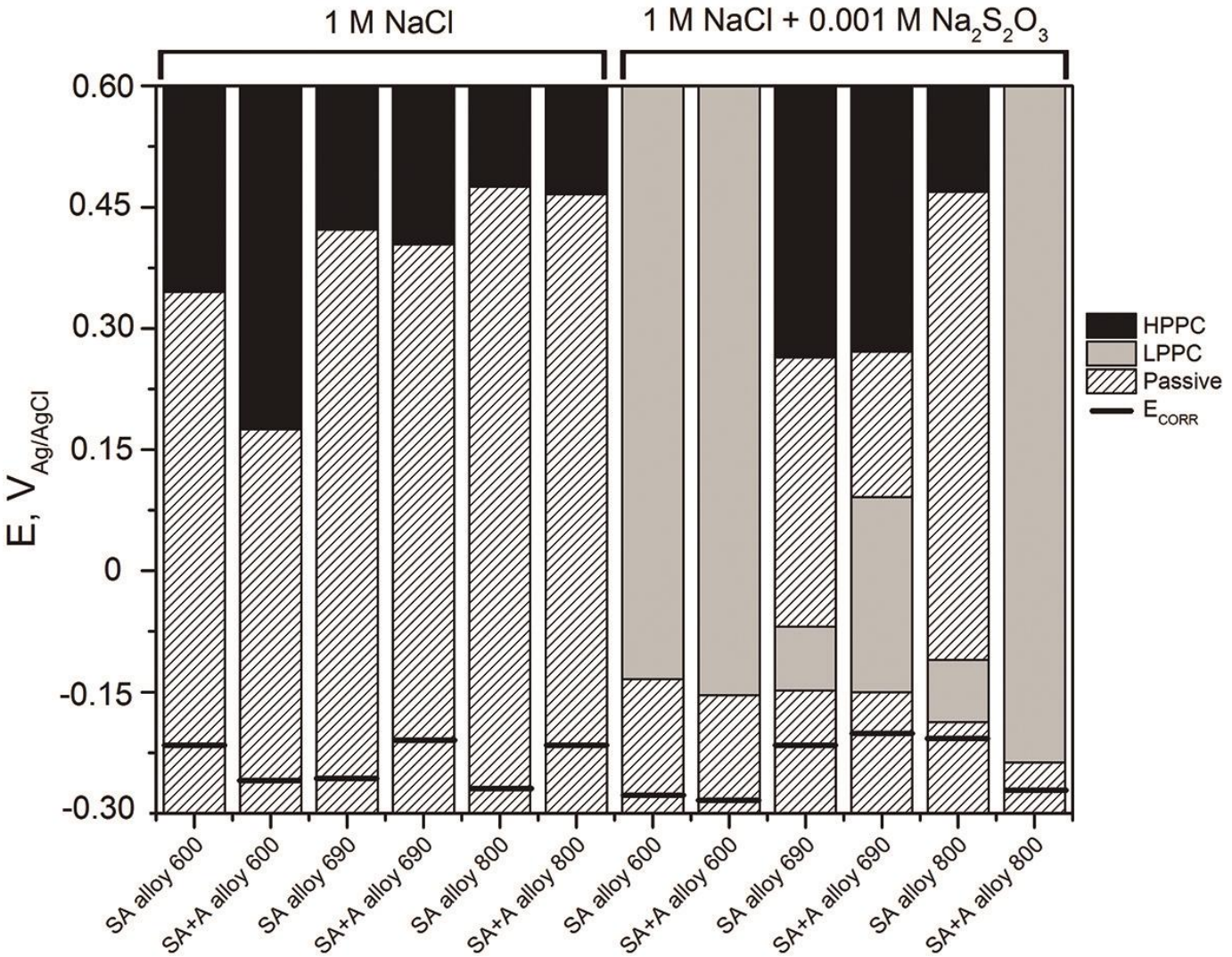

FIGURE 17.Potential ranges associated with passivity and pitting corrosion for tested alloys in 1 M NaCl and 1 M NaCl+ 0.001 M $Na_2S_2O_3$. E_{CORR} values were measured during 1 hour.